JAST
Journal of Aerospace Science and Technology

Pages: 99-118 / Vol. 15/ Issue 1 / Winter- Spring 2022

Journal of Aerospace Science and Technology

www:jast.ias.ir

Scientific-Research Article

Development of Nonlinear Model and Implementation of Real-Time Flight Simulation of a Flexible Projectile in Simulink Environment for Initial Design and Stability Analysis

Hossein Faveadi[1], **Alireza Davari**[2], **Farshad Pazooki**[3], **Majid Pouladian**[44]

1–2-3- Department of Aerospace Engineering, Science and Research Branch, Islamic Azad University
4- Department of Medical Engineering, Science and Research Branch, Islamic Azad University

ABSTRACT

Flight simulation is an efficient tool in testing, evaluation and validation of aircrafts' design by observing flight parameters and predict the results of field tests in order to evaluation of design; In this regard for designing a flexible projectile, a nonlinear model is developed and also is simulated by implementing it in the Simulink environment; In this way, the role of some design parameters or inputs such as: structure's natural frequencies, maneuvering acceleration, propulsion curve, initial or inherent misalignment or deflection of propulsion, angular velocities especially spinning velocity etc. has been examined.

By comparing flexible projectile flight simulation or so-called "Elastic flight simulation" to the "Rigid flight simulation", on issues such as flight behavior, trajectory and collision accuracy, propulsion curve and its initial errors, spinning velocity, effect of the control commands etc., elastic model gives more accurate, reasonable and realistic answer; However, in issues such as the study of the effect of aerodynamic load distribution, stiffness and inertia distribution, structure's natural frequency, etc. only simulations based on elastic model will be able to respond. Accordingly, the main orientation of this research is to develop a model and software tool in order to flight simulation of flexible projectile with acceptable accuracy and high run speed to achieve some of the mentioned goals; However, due to the extent variety of input parameters and their interaction, in this study, only initial misalignment & deflection of propulsion, spin velocity and structure's natural frequency is covered and other cases will be examined in future studies.

Keywords: *Aeroelasticity, Flight simulation, Flexible projectile, Design parameters, Time domain stability analysis*.

Introduction

Aeroelasticity is expressed as the interaction between aerodynamic and structural deformations, which itself is divided into two areas, static and

1 PhD. Candidate
2 Associate Professor (Corresponding Author) **Email: *** ardavari@srbiau.ac.ir
3 Assistant Professor
4 Associate Professor

DOI: 10.22034/jast.2022.246477.1036
Submit: 0310.2020/ Accepted: 30.01.2022
Print ISSN:2345-3648 Online ISSN: 1735-2134

dynamic aeroelasticity; In static aeroelasticity, the role of inertial loads (structural vibrations) on aerodynamic behavior is ignored; But in dynamic aeroelasticity, the role of inertial loads is also effective and the deformation of structures is accompanied by vibration; Aeroelasticity has been studied in many studies and researches, most of them related to destructive and adverse effects of aeroelasticity on instability phenomena such as divergence and flutter and control loop design of flexible aircrafts which is called as aeroservoelasticity. The main methods of aeroelastic analysis in these studies base on linearization of state equations and stability analysis around the equilibrium point or trim flight level. For example, in the first research on aeroelasticity analysis, Kirsch [1] derived the equations of motion for a flexible projectile by using Lagrange equations; Then, by linearizing and transferring them to the steady state space, stability of the flexible projectile was examined; In the same direction, Mierovitch and Nelson [2] used the same equations to study the aeroelastic stability of a high-spin satellite with flexible components; Platus and Segundo [3] investigate about stability and design of controller for the spinning flexible projectile with a slender body; In this study, after obtaining the equations of motion for a projectile, the linearization of equations was extracted around a trim level condition or equilibrium point; In the following, the aerodynamic pressure and the spin velocity that causes the aeroelastic instability of the projectile are extracted.

In most studies on stability analysis of the flexible projectiles, calculations have been performed based on linearized equations of motion and transforming them to steady space; As a result of linearization has neglected the role of nonlinear and coupling expressions; Of course, this linearization does not cause a significant error in aeroelastic instability analysis, because if the linearized equations become unstable, instability will certainly occur in nonlinear equations and consequently in real conditions; But in this way, the allowable ranges for the aerodynamic pressure of the projectile become more limited and the design more conservative in other word the margin of stability decreases [4]; In stability analysis via simulation in time domain, there is no limitation and no requirement for linearization, therefor equations can be fully implemented; But the main weakness of this method is impossibility of achievement to explicit answers; Because instability occurs over time, it is a bit difficult to extract or judge what flight condition caused the instability; It should also be noted that in simulation-based or time-based analyzes, omitting nonlinear or coupling expressions reduces accuracy and is also illogical especially when it is supposed to compare the results of flexible body simulation with rigid type [5].

In studies related to the time domain analysis of aeroelastic instability; Anne Da Silva and colleagues [3] have investigated the aeroelastic stability of sounding rocket; In their research, by simultaneously solving structural and aerodynamic equations by use of Z-Aero software, they have studied the stability of a flexible rocket and determined the instability velocity of the flutter; In this study flutter analysis was done according to generalized time function from modal approach; It has also been shown that as the rolling speed increases, the aerodynamic pressure required for the flutter decreases and the stability domain becomes smaller.

The results of flexible projectile simulation are not limited to stability analysis and can be used in other areas such as control loop design and evaluation, primary design (modification or optimization), navigation devices' position placement and improvement coincidence of simulations' result with the field tests. The design optimization and improvement coincidence of simulations' results with the field tests (achieving more realistic results) have been investigated in this research; In practice, the use of simulation in the fields of design and optimization, especially during the conceptual and primary stage of design, is considered more than other fields such as stability analysis; For example, in a study conducted by the Elyada [4], the effects of stiffness distribution and aerodynamic geometry and their role on the aeroelastic stability of the projectile were investigated and evaluated, and finally the better configuration was selected. Of course, this design optimization is not done with the help of simulation in the time domain, but based on the method of linearization of state equations and extraction of divergence velocity and flutter; However, in this study, in addition to study of the flight stability, by comparing flight quantities in two rigid and flexible simulations and finding the causes, the optimal selection of design parameters is also done; In this regard, it is obvious that the closer the simulation results are to the results of field tests, the better and more accurate evaluation of the aircraft can be.

In guided or controlled projectiles, flexibility can affect the stability of control loop and controlling effort, accuracy of the collision, circular error probable (CEP) etc.; Control commands usually significantly increase the loads on the structure instantly, thus increasing the effects of structural flexibility; These effects can have on issues such as flight path, collision accuracy, command following, controlling effort, design and selection of guidance law and many similar issues that are beyond the scope of this study, but can be considered in future studies. However, in this study, a few control commands have been applied in order to investigate the role of structural flexibility to show the reader how changes in applied loads affect the aeroelastic response of the structure and what measures can be taken in this regard; It also can be shown how these commands, along with cumulative factors such as inherent deflection of the propulsion force and rolling speed, increase flight path mismatch and the probability of flexible projectile instability.It also can be shown that how these commands, along with cumulative factors such as inherent deflection of the propulsion force and rolling speed, increase flight path mismatch and the probability of flexible projectile instability. In these circumstances to prevent these adverse effects it is necessary to increase natural frequency of the structure or modify design parameters. In this regard, it is shown that in a unguided projectile with a conventional design (slenderness ratio less than 15 with structural thicknesses of a few millimeters) aeroelastic effects rarely cause flight instability; Because in practice, due to the large diameter (due to embedding requirements of parts & subsystems) and high thickness (due to requirements for production and jointing of bays), the rigidity of the structure and thus its natural frequency will be high (More than 20 Hz for first frequency); Therefor in absence of the control commands, flexibility just cause changing in flight quantities and accuracy in the flight path of the projectile rather than its instability.

Extraction equations of motion

Due to the infinite degrees of flexibility of the flexible projectile, the Lagrangian relation is used to derive the equations of motion; In this method, generalized quantities or coordinates, kinetic energies, potentials and depreciation are used to derive equations of motion. The form of Lagrange equations is as follows [5].

$$\frac{d}{dt_B}\left(\frac{\partial T}{\partial \dot{q}_i}\right)^T - \frac{\partial T}{\partial q_i} + \frac{\partial U}{\partial q_i} + \frac{\partial D}{\partial \dot{q}_i} = Q_{q_i} \qquad (1)$$

In the above relation, q_i: represents the generalized coordinates or state parameters, T: kinetic energy, U: potential energy, D: Damping or dissipation energy and Q_{q_i}: generalized load in the direction of the generalized coordinate Q_i; In order to calculate the quantities used in Lagrange equations, it is first necessary to determine the position vector of the material element of the body ($\vec{R}$) relative to a fixed reference i.e. ground reference; In this regard, it is assumed that each vector that connected material element to body`s center of mass consists of a rigid part $\overrightarrow{r_o}$ and a non-rigid or elastic part ($\vec{e}$) (see Figure 1). $\vec{r}$: is also a vector that connects the fixed reference to the center of mass of the flexible projectile [6].

$$\vec{E} = \vec{R} + \vec{r} \qquad (2)$$

$$\vec{r} = \overrightarrow{r_o} + \vec{e} \qquad (3)$$

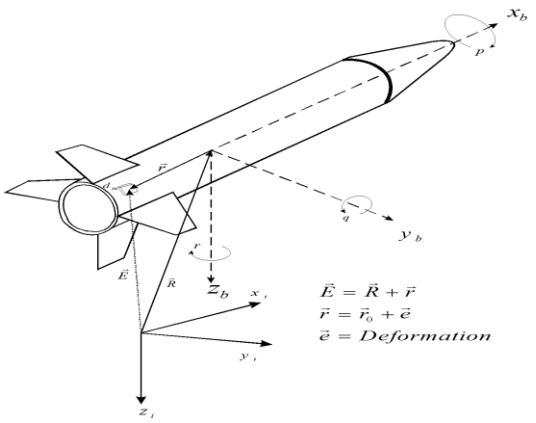

Figure 1 Schematic configuration of coordinate and vectors related to the mass element of a flexible projectile.

The elastic component of the position vector ($\vec{e}$) is calculated based on the deformation behavior of the projectile in a form of transverse bending vibration in two $x-y$ and $x-z$ planes, which is consistent with the fact that the major aerodynamic loads and guidance commands apply in these directions; Accordingly, the effects of torsional and longitudinal vibrations of the structure in comparison with transverse vibrations are neglected. The structural deformation vector $\vec{e}$ can be written as follows using harmonic analysis and the "assumed modes" method [6]:

$$\vec{e}(x,t)=\begin{Bmatrix}0\\e_y(x,t)\\e_z(x,t)\end{Bmatrix}=\begin{Bmatrix}0\\\sum_{j=1}^{N_e}\phi_i(x)\eta_i(t)\\\sum_{j=1}^{N_e}\phi_i(x)\xi_i(t)\end{Bmatrix} \quad (4)$$

In the above relation, $\phi_i(x)$: indicates the transverse vibration mode shapes or generalized function of the flexible projectile; Also, $\eta_i(t)$ and $\xi_i(t)$ represent time functions or generalized coordinates, respectively in the $x-y$ and $x-z$ planes corresponding to these vibrations; Due to the high slenderness ratio of the projectile (ratio of its length to diameter), its structure is considered as a Euler-Bernoulli beam (the effect of shear deformation is ignored) with the effects of axial force N (x) (by considering the effect of axial force on changing the natural frequency of the structure), Taken from following equation: [7]

$$m(x)\frac{\partial^2\delta(x,t)}{\partial t^2}+\frac{\partial^2}{\partial x^2}\left[\mathrm{E}(x)\mathrm{I}_{zz}(x)\frac{\partial^2\delta(x,t)}{\partial x^2}\right]+\frac{\partial}{\partial x}\left[\mathrm{N(x)}\frac{\partial\delta(x,t)}{\partial x}\right]=0$$

Which $\delta(x,t)$: represent the transverse deformation, $E\,(x)$: is the Young's modulus distribution and $I\,(x)$: is the second moment of inertia of the projectile's structure; The spatial function $\phi_i(x)$ is calculated based on (Equation 5) and according to the boundary conditions of the two free ends:

$$m(x)\omega_i^2\phi_i(x)+\frac{\partial^2}{\partial x^2}\left[\mathrm{E}(x)\mathrm{I}_{zz}(x)\frac{\partial^2\phi_i(x)}{\partial x^2}\right]x+\frac{\partial}{\partial x}\left[\mathrm{N(x)}\frac{\partial\phi_i(x)}{\partial x}\right]=0 \quad (6)$$

ω_i: is the natural frequency of the projectile corresponding to each vibration mode; Frequencies and mode shapes is determined by the by numerical or approximate methods like Galerkin method which can validated by modal experimental test.

The Lagrangian equations is written in the body coordinate (aligned with center of mass of the flexible projectile) and the derivative of the flight quantities relative to the bare or stationary apparatus is calculated using Coriolis law [6] and [3] If the velocity vector of the center of the body apparatus and the velocity vector of each component in the absolute apparatus are equal to $\overrightarrow{V_t}=\frac{d\vec{E}}{dt_I}$ and $\overrightarrow{V_o}=\frac{d\vec{R}}{dt_I}$ are displayed, then after deriving relations (2) and (3) and using the law of Coriolis, the velocity of each mass component is written as follows [3]:

$$V_i=V_o+\frac{d\overrightarrow{r_o}}{dt_B}+\frac{d\vec{e}}{dt_B}+\omega_{I/B}\times(\overrightarrow{r_o}c\ +\vec{e}) \quad (7)$$

$\omega_{I/B}$: Indicates the angular velocity of the inertial coordinate system relative to the body coordinate or the values of the angular velocity of the projectile (P,Q,R); The expression $\frac{dr_o}{dt_B}$: represents the linear velocity vector of the projectile in the body system or the same expression (U, V, W); $\overrightarrow{r_o}$: which represents the rigid portion of body vector of position ($\overrightarrow{r_o}=\begin{Bmatrix}x\\y\\z\end{Bmatrix}$); Obviously, the time derivative of this vector is zero, ie ($\frac{dr_o}{dt_B}=0$, the expression ($\frac{d\vec{e}}{dt_B}$) also means the strain rate of the projectile material particles; By placing the values in Equation (7), the following relation is obtained for the velocity of each material particle of the flexible projectile:

$$V_i=\begin{Bmatrix}U+Qz-Ry\\V+Rx-Pz\\W+Py-Qz\end{Bmatrix}_R+\begin{Bmatrix}Q\sum_{i=1}^{N_e}\phi_i\xi_i-R\sum_{i=1}^{N_e}\phi_i\eta_i\\\sum_{i=1}^{N_e}\phi_i\dot{\eta}_\iota-P\sum_{i=1}^{N_e}\phi_i\xi_i\\\sum_{i=1}^{N_e}\phi_i\dot{\xi}_i+P\sum_{i=1}^{N_e}\phi_i\eta_i\end{Bmatrix}_E \quad (8)$$

Given that in the simulation of a flexible projectile flight, it is desirable to compare the share of rigid and elastic expressions, so in Equation (8), the share of rigid and elastic expressions is distinct with the help of R and E indexes respectively; According to (Equation 8), it can be argued that the flexibility effects are more significant for projectiles with high values of angular velocities, which is shown in the section on simulation results.

Kinetic energy

The kinetic energy is calculated from the total kinetic energy of the mass components (lumped or continues) with respect to the velocity of each of them (Equation 7); The general relation of the

calculation of kinetic energy in terms of the general vector mass element could be written as follows [8]:

$$T = \frac{1}{2}\int \frac{d\vec{E}}{dt_I}.\frac{d\vec{E}}{dt_I}dm = \frac{1}{2}\int \vec{V_l}.\vec{V_l}dm \quad (9)$$

By replacing Equation (7) in Equation (9), the general relation of the kinetic energy for the flexible projectile is obtained as Equation (10); Again, by separating the contribution of elastic terms, the role of structural deformation can be seen more clearly in the kinetic energy of the projectile and it can be used to study and analyze the stability of the flexible projectile in the absence of external excitation or control loads.

$$T = T_R + T_E$$

$$T_R = \frac{1}{2}M(U^2+V^2+W^2) + \frac{1}{2}\left[I_{xx}(Q^2+R^2) + I_{yy}(P^2+R^2) + I_{zz}(P^2+Q^2)\right]$$

$$T_E = \frac{1}{2}\sum_{i=1}^{N_e} m_i(\dot{\eta}_i^2+\dot{\xi}_i^2) + P\sum_{i=1}^{N_e} m_i(\eta_i\dot{\xi}_i - \dot{\eta}_i\xi_i) - QR\sum_{i=1}^{N_e} m_i\eta_i\xi_i + \frac{1}{2}(P^2+R^2)\sum_{i=1}^{N_e} m_i\eta_i^2 + \frac{1}{2}(P^2+Q^2)\sum_{i=1}^{N_e} m_i\xi_i^2 \quad (10)$$

m_i: Indicates the generalized mass corresponding to each vibration mode and is calculated from the following relation:

$$m_i = \int_l \phi_i(x)m(x)\phi_i(x)dx \quad (11)$$

From Equation (10), it is clear that the rolling velocity (P) plays a major role in the kinetic energy content of related to flexibility, and as it increases, it is expected that the difference between the two rigid and flexible simulation quantities and possibility of instability increases, which is mentioned in the results section.

Potential energy

The potential energy is an indeterminate quantity, and when the excitation mode of the system is rigid, its value is zero, so the potential energy is only the result of the deformation of the structure; The relation of calculating the potential energy due to the flexural deformation of the structure is as follows [8]:

$$U_e = \frac{1}{2}\int_l \frac{\widehat{M}^2}{2E(x)\mathrm{I}(x)}dx = \frac{1}{2}\int_l E(x)\mathrm{I}(x)\left(\frac{d^2\delta(x,t)}{dx^2}\right)^2 dx \quad (12)$$

Which in the above equation, $\widehat{M}$: is the flexural moment distribution along the projectile structure; According to the relationship between flexural moment and deformation, Equation (12) can be written as follows:

$$U_e = \frac{1}{2}\int_l E(x)\mathrm{I}_{yy}(x)\left(\frac{d^2e_y}{dx^2}\right)^2 + E(x)\mathrm{I}_{zz}(x)\left(\frac{d^2e_z}{dx^2}\right)^2 dx \quad (13)$$

Assuming the radial symmetry of the structure's properties and the mass distribution, the second surface inertia distribution on the $x-y$ and $x-z$ planes can be equalized, ie: $I_{yy} = I_{yy} = I$, which is finally replaced by the expression the deformations of e_y And e_z (Equation 4) The following equation is extracted:

$$U_e = \frac{1}{2}\sum_{j=1}^{N_e} k_{e_i}(\eta_i^2+\xi_i^2) = \frac{1}{2}\sum_{j=1}^{N_e} m_i\omega_i^2(\eta_i^2+\xi_i^2) \quad (14)$$

k_{e_i}: Indicates the generalized equivalent stiffness that is calculated from the following equation:

$$k_{e_i} = k_{str_i} + k_{N_i} = \int_l \frac{\partial^2}{\partial x^2}(\phi_i(x)\mathrm{E}(x)\mathrm{I}_{zz}(x))\frac{\partial^2\phi_i(x)}{\partial x^2}dx + \int_l \frac{\partial}{\partial x}(\phi_i(x)\mathrm{N}(x))\frac{\partial\phi_i(x)}{\partial x}dx \quad (15)$$

k_{str_i}: is stiffness related to the mechanical characteristics of projectile's structure and k_{N_i}: is the share or effect of the axial force in changing of the projectile's stiffness; Obviously, the expression for potential energy (14) is only consist of elastic quantities, and therefore its effect will appear only in Vibration equations of the projectile.

Damping energy

Damping energy reduces the vibrational energy of the projectile; Although the contribution of this energy is not regardable for integrated metal structures compared to kinetic and potential, it has been modeled due to the conceptual design and its role in body dynamics; The amount of energy dissipation for a continuous vibration system can be calculated as follows [8]:

$$D = \frac{1}{2}\int_L C(x)\frac{d\delta(x)}{dt_B}.\frac{d\delta(x)}{dt_B}dx = \frac{1}{2}\int_L \frac{C(x)}{\rho(x)A(x)}\frac{d\delta(x)}{dt_B}.\frac{d\delta(x)}{dt_B}dm \quad (16)$$

In the above relation, the value of C (x), represents distribution of damping coefficient, $\rho(x)$: represents density per unit length of the projectile and $A(x)$: represents the cross-sectional distribution of the structure contributes sustaining loads. By Using the orthogonality of vibration modes, the relation of dissipative energy is written as follows:

$$D = \sum_{j=1}^{N_e} \mu_i m_i \omega_i (\eta_i + \xi_i) \quad (17)$$

In the above relation, μ_i: is specific dumping related to each vibration mode; Its exact value can be obtained from the experimental modal method; But its normal value can be considered for almost uniform aluminum structures (about 0.01 to 0.02) for the first mode and about 00.05 to 0.002 for the second mode and its effect can be ignored in higher modes.

Extraction of equations of motion for flexible projectile

By placing the amount of kinetic energy (Equation 10), potential energy (Equation 14) and depreciation energy (Equation 17) in the Lagrange equations (1), the projectile motion equations are obtained; The first three equations (12-20) are related to the transient motion and the second three equations (23-21) are related to the rotational motion of the projectile and the two sets of equations (24 and 25) are related to the transverse vibrations of the projectile which are considered according to the number of vibration modes Taken, it contains the same number of independent equations.

$$\dot{U} = \frac{F_x}{M} + \left[RV - QW - \acute{M}U\right]_R \quad (18)$$

$$\dot{V} = \frac{F_y}{M} + \left[PW - RU - \acute{M}V\right]_R \quad (19)$$

$$\dot{W} = \frac{F_z}{M} + \left[QU - PV - \acute{M}W\right]_R \quad (20)$$

$$\dot{P} = \frac{1}{I_{xx} + \sum_{i=1}^{N_e} m_i(\eta_i^2 + \xi_i^2)}\left[M_x - \dot{I}_x P + \left(\sum_{i=1}^{N_e} m_i(\ddot{\eta}_i\xi_i - \eta_i\ddot{\xi}_i) + (Q^2 - R^2)\sum_{i=1}^{N_e} m_i\eta_i\xi_i - 2P\sum_{i=1}^{N_e} m_i(\eta_i\dot{\eta}_i + \xi_i\dot{\xi}_i) + QR\sum_{i=1}^{N_e} m_i(\xi_i^2 - \eta_i^2)\right)_E\right] \quad (21)$$

$$\dot{Q} = \frac{1}{I + \sum_{i=1}^{N_e} m_i\xi_i^2}\left[M_y - \dot{I}Q + PR(I - I_{xx}) + \left(-PR\sum_{i=1}^{N_e} m_i\xi_i^2 + (\dot{R} - PQ)\sum_{i=1}^{N_e} m_i\eta_i\xi_i - 2Q\sum_{i=1}^{N_e} m_i\xi_i\dot{\xi}_i + 2R\sum_{i=1}^{N_e} m_i\dot{\eta}_i\xi_i\right)_E\right] \quad (22)$$

$$\dot{R} = \frac{1}{I + \sum_{i=1}^{N_e} m_i\eta_i^2}\left[M_z - \dot{I}R - PQ(I - I_{xx}) + \left(PQ\sum_{i=1}^{N_e} m_i\eta_i^2 + (\dot{Q} + PR)\sum_{i=1}^{N_e} m_i\eta_i\xi_i - 2R\sum_{i=1}^{N_e} m_i\eta_i\dot{\eta}_i + 2Q\sum_{i=1}^{N_e} m_i\eta_i\dot{\xi}_i\right)_E\right] \quad (23)$$

$$\ddot{\eta}_i = \frac{Q_{\eta_i}}{m_i} - 2\mu_i\omega_i\dot{\eta}_i + (P^2 + R^2 - \omega_i^2)\eta_i + 2P\dot{\xi}_i + (\dot{P} - QR)\xi_i \quad (24)$$

$$\ddot{\xi}_i = \frac{Q_{\eta_i}}{m_i} - 2\mu_i\omega_i\dot{\xi}_i + (P^2 + Q^2 - \omega_i^2)\xi_i - 2P\dot{\eta}_i - (\dot{P} + QR)\eta_i \quad (25)$$

In the above phrases, M´: indicates the ratio of the mass rate to initial mass of the projectile, ie: $(\frac{\dot{M}}{M})$ and $\dot{I}$: also indicates the rate of changing of rotational inertia of the projectile relative to the y or z axes; The rate of the axial rotational inertia ($\dot{I}_{xx}$) is also ignored. In all equations, the share of rigid and elastic expressions in linear and angular velocities is specified; In the equations of transition velocity, the direct role of flexibility can be eliminated with a few simplistic assumptions; But in angular velocity equations, the role of flexibility is obvious and indelible; It is also observed that flexibility gives rise to new expressions or quantities that could not be observed in rigid simulation at all; For example the values: $\sum_{i=1}^{N_e} m_i\xi_i^2$ and $\sum_{i=1}^{N_e} m_i\eta_i^2$ Which is interpreted as elastic rotational inertia, causes the dependence or overlap of rigid and elastic expressions in equations of angular velocity; It is also obvious that all the sentences related to the transverse vibrations (equations 24 and 25) contain the generalized coordinates η_i and ξ_i; The number of vibrational equations in each transverse plane is equal to the number of considered mode shapes.

Distribution of the wind-body angles

In order to calculate aerodynamic loads, it is first necessary to determine the distribution of the wind-body angles; Unlike the rigid model, the angles of attack and side-slip in the flexible projectile will be variable on geometry of the projectile due to its deformations and vibrations; According to the definition of these angles, their distribution can be expressed as follows:

$$\alpha_e(x,t) = \left[\alpha_r - \frac{Qx_l(x)}{V_\infty}\right]_R + \frac{1}{V_\infty}\left[\sum_{i=1}^{\infty}\phi_i(x)\dot{\xi}_i(t) + \frac{P}{V_\infty}\sum_{i=1}^{\infty}\phi_i(x)\eta_i(t) - \sum_{i=1}^{\infty}\acute{\phi}_i(x)\xi_i(t)\right]_E \quad (26)$$

$$\beta_e(x,t) = \left[\beta_r + \frac{Rx_l(x)}{V_\infty}\right]_R + \frac{1}{V_\infty}\left[\sum_{i=1}^{\infty}\phi_i(x)\,\dot{\eta}_i(t) - \frac{P}{V_\infty}\sum_{i=1}^{\infty}\phi_i(x)\xi_i(t) - \sum_{i=1}^{\infty}\acute{\phi}_i(x)\eta_i(t)\right]_E \quad (27)$$

In the above relation $x_l(x)$: denotes the distance from the each body element to the current C.G. of the projectile, $\left[\alpha_r - \frac{Qx_l}{V_\infty}\right]_R$ and $\left[\beta_r + \frac{Rx_l}{V_\infty}\right]_R$ are the rigid portion to the angle of attack and the side-slip respectively and expressions related to flexibility are indicated by footnote E; It should be noted that the rigid components just means the similarity of the calculation with the rigid state and the non-direct dependence on the deformation of the structure.

Estimation and calculation of aerodynamic loads

Due to the use of the body coordinate in extracting the equations of motion, it is necessary to express the aerodynamic coefficients and loads in the same coordinate instead of the stability coordinate; Another reason for this is the effect of aerodynamic coefficients from deformation and vibration of the body. The quasi-stable method is used to calculate aerodynamic loads in the sense that the aerodynamic coefficients or their distribution are multiplied by the instantaneous values of the wind-body angle distribution; This assumption is valid for the case where the natural frequency of the body is very different from the minimum frequency of aerodynamic loads; For this purpose, the deformations of the structure must also be in the linear ranges; The general relation for calculating aerodynamic loads is as follows:

$$F_{A_x}, F_{A_y}, F_{A_z} = Q_\infty S_{ref}(C_x, C_y, C_z \quad (28)$$

$$M_{A_x}, M_{A_y}, M_{A_z} = Q_\infty S_{ref} d(C_l, C_m, C_n) \quad (29)$$

C_x, C_y, C_z are the aerodynamic force coefficients and C_l, C_m and C_n are the aerodynamic moment coefficients, all of which are expressed in the body system; Q_∞: represents the aerodynamic pressure and S_{ref}: represents the reference aerodynamic surface, which is equal to the cross-sectional area of the projectile; Subtitle A: also represents aerodynamic forces and moments; Due to the changes in wind-body angles during the projectile due to the deformation of the body, the distribution of aerodynamic coefficients should be used instead of their constant values. In general, the relation for calculating aerodynamic loads is as follows:[۸]

$$C_x = \int_0^l \left(C_{x_\beta}(x)\beta(x) + C_{x_\alpha}(x)\alpha(x)\right) dx + C_{x_0} + C_{x_p} p \frac{d}{2V} + C_{x_\delta}\delta \quad (30)$$

$$C_y = \int_0^l \left(C_{y_\beta}(x)\beta(x) + C_{y_{\dot\beta}}(x)\dot\beta(x)\right) dx + C_{y_r} r \frac{d}{2V} + C_{y_{\delta r}}\delta_r \quad (31)$$

$$C_Z = \int_0^l \left(C_{z_\alpha}(x)\alpha(x) + C_{z_{\dot\alpha}}(x)\dot\alpha(x)\right) dx + C_{z_q}(x) q \frac{d}{2V} + C_{z_{\delta e}}\delta e \quad (32)$$

$$C_l = \int_0^l \left(C_{l_\alpha}(x)\alpha(x) + C_{l_\beta}(x)\beta(x)\right) dx + C_{l_0} + C_{l_p} p \frac{d}{2V} + C_{l_{\delta a}}\delta a \quad (33)$$

$$C_m = \int_0^l \left(C_{m_\alpha}(x)\alpha(x) + C_{m_{\dot\alpha}}(x)\,\dot\alpha(x)\right) dx + C_{m_0} + C_{m_q} q \frac{d}{2V} + C_{m_{\delta e}}\delta e \quad (34)$$

$$C_n = \int_0^l \left(C_{n\beta}(x)\beta(x) + C_{n_{\dot\beta}}(x)\dot\beta(x)\right) dx + C_{n_0} + C_{n_r} r \frac{d}{2V} + C_{n_{\delta r}}\delta r \quad (35)$$

Due to the geometry and flight conditions, not all aerodynamic coefficients have the same effect and importance, and some coefficients such as: $C_{Z_{\dot\alpha}}$ and $C_{y_{\dot\beta}}$ can be compared with the role of coefficients. C_{Z_α} and C_{y_β} ignored; But in this regard, it is necessary to pay attention to the value of the wind-body angle rates in comparison with their own value; Most aerodynamic moment coefficients are not independent coefficients and are obtained by integrating the force coefficients relative to the projectile's C.G (relationships 36 to 38); In order to validation in calculations related to the distribution of aerodynamic coefficients, the integral obtained from the distribution of aerodynamic coefficients must be equal to their single values used in rigid body simulation.

Also, if the effects of angular velocities in the wind-body angular distribution is considered as $\frac{Qx_l}{V_\infty}$ and $\frac{Rx_l}{V_\infty}$ then the aerodynamic coefficients: C_{z_q}, C_{y_r}, C_{n_r} and C_{m_q} should be eliminate in aerodynamic load calculations, or by keeping them and remove $\frac{Qx_l}{V_\infty}$ and $\frac{Rx_l}{V_\infty}$ from the wind-body angle distribution. In order to calculation validation of the distribution of the aerodynamic coefficients, the integrals obtained from the distribution of aerodynamic coefficients must be equal to their single values, which are used in rigid simulations.

$$C_{l_\alpha} = \int_0^l C_{x_\alpha}(x) x_l dx \;\&\; C_{l_\beta} = \int_0^l C_{x_\beta}(x) x_l dx \quad (36)$$

$$C_{m_\alpha} = \int_0^l C_{z_\alpha}(x) x_l(x) dx \;\&\; C_{m_q} = \int_0^l C_{z_q}(x)\, x_l(x) dx \;\&\; C_{z_q} = \frac{2}{d}\int_0^l C_{z_\alpha}(x)\, x_l(x) dx \quad (37)$$

$$C_{n_\beta} = \int_0^l C_{y_\beta}(x) x_l(x) dx \;\; \& \;\; C_{n_r}$$
$$= \int_0^l C_{y_r}(x)\, x_l(x) dx \;\; \& \;\; C_{y_r} \qquad (38)$$
$$= \frac{2}{d} \int_0^l C_{y_\beta}(x)\, x_l(x) dx$$

The required aerodynamic coefficients are also calculated by using Missile Datcom (MD) software or Ansys-Fluent software with same meshing which is used to calculate the wind-body angle distribution; The distribution of coefficients and their integral values are confirmed in advance with the help of experimental wind tunnel test and the use of barometers in different parts of the body; The coefficients that are considered without distribution along the body are called rigid aerodynamic coefficients, like: C_{l_0}, C_{m_0}, C_{n_0}, C_{z_q}, C_{x_q} ,C_{l_r} ,C_{l_p}, C_{y_p} etc. These coefficients are largely independent of the distribution of wind-body angles and can be in called from look up tables of rigid (non-distributive) values; As mentioned, other coefficients in aerodynamic moment (such as C_{n_β} and C_{m_α}) are also calculated indirectly by weighting from the distribution of the force aerodynamic coefficients relative to projectile's C.G. according to relations (36) to (38).

In order to perform calculations related to aerodynamic loads (30) to (35) during simulation, the values of wind-body angle distribution α (x) and β (x) are replaced and multiply in the aerodynamic pressure and the reference surface area. The distribution of aerodynamic coefficients and wind-body angles should be determined, depending on different flight conditions and the body deformations at each time step of the simulation; This is a time-consuming process and impairs the real-time capability of the simulation; To solve this problem, the distribution of aerodynamic coefficients and their multiplication in expressions such as vibration modes (used in the calculation of generalized loads) are precalculated based on meshed geometry (Figure 3-a) and imported as look-up tables in the simulation code; Therefore, according to the number of elements and vibration modes, the dimension of aerodynamic coefficient look-up tables is increased.

During simulation, required data only are called according to the element number, mode number and related aerodynamic conditions, including: wind-body angles values, Mach and Reynolds numbers. This process is used in calculations of aerodynamic loads, generalized loads, and wind-body angle distributions; With this solution, the simulation execution speed (run speed) is significantly increased and the ability to execute real-time and use in projectile flight computer is provided. (Figure 3-b.

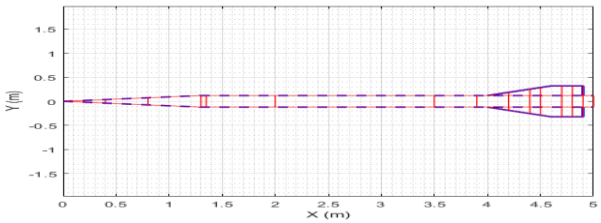

Figure 3-a shows the meshing performed on the external geometry of the projectile in order to calculate the distribution of aerodynamic loads & equivalent wind-body angles.

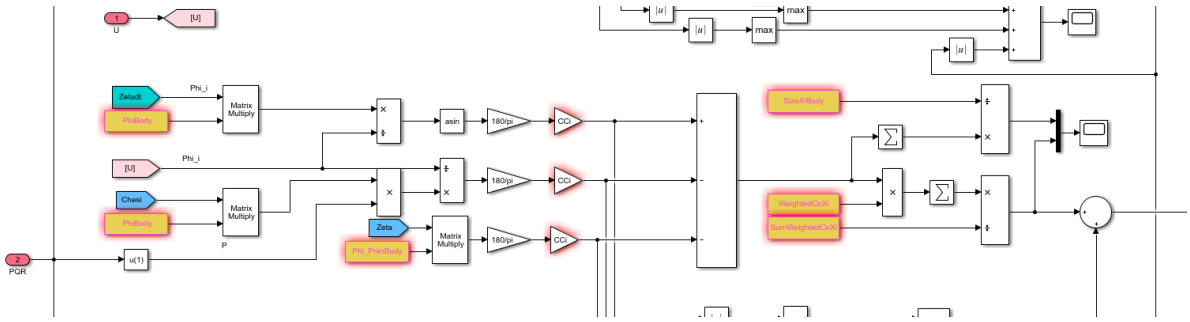

Figure 3-b shows a section from the block diagram related to calculating of the angle-body distribution during flight simulation in which predefined values (yellow rectangular blocks) are used to reduce volume of running calculations and thus increase the simulation speed

Deflection of the propulsion due to body's deformations

Due to the presence of initial or inherent deflection (decentralization and angular deviation) as well as flexural deformation (transverse deformation and inclination at the exit of the propulsion), the components of the propulsion vector change, which ultimately creates unwanted forces and moments for the projectile; Inherent deviations in the propulsion can be considered as fixed or random values with a certain standard deviation, each of which can correspond to reality according to the conditions of simulation; In this study, a constant value is considered for the inherent error of the propulsion. The components of the propulsion vector due to the inherent deflection and deformation of the body in the position of applying this force to the body are calculated as follows: [9]

$$F_{T_{Deviation}} = \begin{Bmatrix} \cos\theta_{T_{x-y}} \cos\theta_{T_{x-z}} \\ \sin\theta_{T_{x-y}} \cos\theta_{T_{x-z}} \\ -\sin\theta_{T_{x-z}} \end{Bmatrix} F_{Trust} \quad (39)$$

In the above relation, F_{Trust}: is magnitude of the propulsion vector, $\theta_{T_{x-y}}$ and $\theta_{T_{x-z}}$: respectively, represent the angles of deflection of the propulsion vector due to inherent and deflection cause by body deformation in xy and xz planes, which are calculated as follows:

$$\theta_{T_{x-y}} = \theta_{I_{x-y}} + \theta_{\eta_e} \qquad \theta_{T_{x-z}} = \theta_{I_{x-z}} + \theta_{\xi_e} \quad (40)$$

In the above relation ($\theta_{I_{x-y}}$, $\theta_{I_{x-z}}$) and (θ_{η_e} , θ_{ξ_e}) represent the angles, respectively inherent deflection (from initial angular error) and elastic deflection (from body deformation) of propulsion in planes xy and xz; The elastic deflection angle is calculated as follows:

$$\theta_{\eta_e}(t) = \sum_{i=1}^{\infty} \dot{\phi}_i(x_{thrust})\eta_i(t) \qquad \theta_{\xi_e}(t) = \sum_{i=1}^{\infty} \dot{\phi}_i(x_{thrust})\xi_i(t) \quad (41)$$

In the above relation $\dot{\phi}_{i_{x_{thrust}}}$: represents the spatial derivative or slope of the mode shape function at the output location of the propulsion vector; By placing relation (38) in relation (47) and then in relation (46), the components of the propulsion vector due to inherent deviation and deformation of the body are obtained as follows:

$$F_{T_{Deviation}} = \begin{Bmatrix} \cos(\theta_{I_{x-y}} + \sum_{i=1}^{\infty} \dot{\phi}_i(x_{thrust})\eta_i(t)) \cos(\theta_{I_{x-z}} + \sum_{i=1}^{\infty} \dot{\phi}_i(x_{thrust})\xi_i(t)) \\ \sin(\theta_{I_{x-y}} + \sum_{i=1}^{\infty} \dot{\phi}_i(x_{thrust})\eta_i(t)) \cos(\theta_{I_{x-z}} + \sum_{i=1}^{\infty} \dot{\phi}_i(x_{thrust})\xi_i(t)) \\ -\sin(\theta_{I_{x-z}} + \sum_{i=1}^{\infty} \dot{\phi}_i(x_{thrust})\xi_i(t)) \end{Bmatrix} T \quad (42)$$

In order to calculate the moment due to the deflection of the propulsion, it is necessary to measure the position of the propulsion force relative to the current projectile's C.G.; Obviously, due to the body's deformation, the value of this vector changes during flight; The position vector of the propulsion relative to the C.G. is calculated according to Equation (40) at each instant of the simulation:

$$r_{T_{Deviation}} = \begin{Bmatrix} x_{thrust} \\ \Delta_{T_{x-y}} + \sum_{i=1}^{\infty} \phi_i(x_{thrust})\eta_i \\ \Delta_{T_{x-z}} + \sum_{i=1}^{\infty} \phi_i(x_{thrust})\xi_i \end{Bmatrix} \quad (43)$$

In the above relation, x_{thrust}: is the position of the propulsion output vector relative to the center of mass, $\Delta_{T_{x-y}}$ and $\Delta_{T_{x-z}}$, respectively, are the inherent out-centering of the propulsion vector relative to the planes xy and xz. Finally, by multiplying the position vector by the propulsion vector, the moment due to the deflection of the propulsion vector is calculated.

$$M_{T_{Deviation}} = r_{T_{Deviation}} \times F_{T_{Deviation}} \qquad (43)$$

The result of this multiplication, which produces the propulsion moment components due to the inherent deflection and deformation of the body, is as follows:

$$F_{T_{Deviation}} = \begin{Bmatrix} \cos(\theta_{I_{x-y}} + \sum_{i=1}^{\infty} \dot{\phi}_i(x_{thrust})\eta_i(t)) \cos(\theta_{I_{x-z}} + \sum_{i=1}^{\infty} \dot{\phi}_i(x_{thrust})\xi_i(t)) \\ \sin(\theta_{I_{x-y}} + \sum_{i=1}^{\infty} \dot{\phi}_i(x_{thrust})\eta_i(t)) \cos(\theta_{I_{x-z}} + \sum_{i=1}^{\infty} \dot{\phi}_i(x_{thrust})\xi_i(t)) \\ -\sin(\theta_{I_{x-z}} + \sum_{i=1}^{\infty} \dot{\phi}_i(x_{thrust})\xi_i(t)) \end{Bmatrix} T \qquad (44)$$

Block diagram of calculations related to the force and moment caused by the deflection of the propulsion is shown in the following figure:

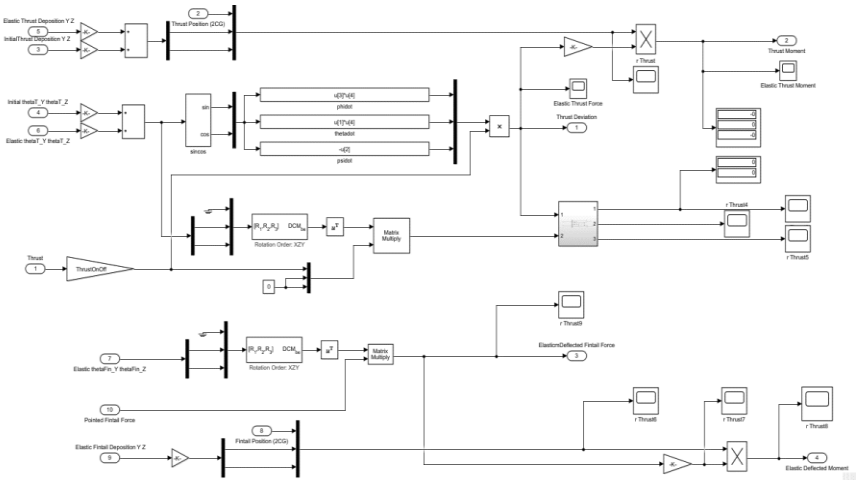

(4-A)

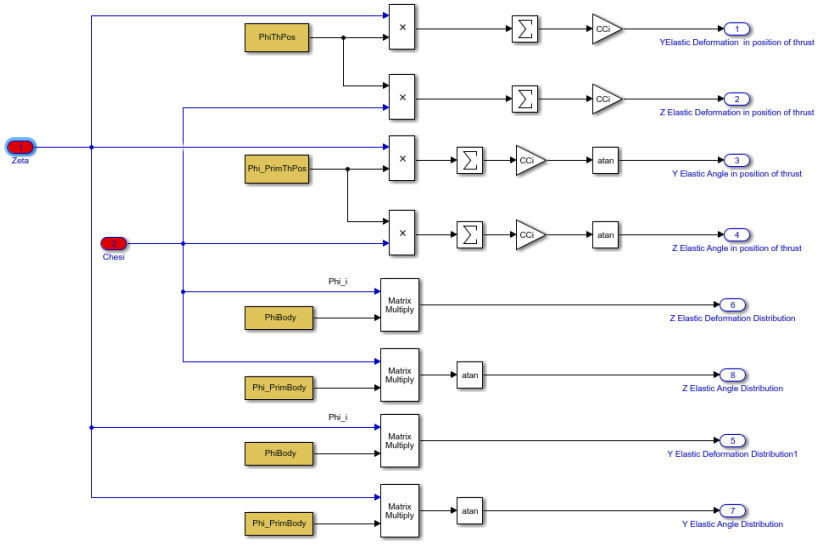

(4-B)

Figure 4 Blocks related to calculations of elastic deflection of propulsion & control surfaces (a); Block diagram of calculating forces and moments due to propulsion deflection(a), elastic deflection of control surfaces (b).

Orientation and positioning

By transferring angular velocities from the body to the inertia coordinate and then integrating from them, the position and orientation of the projectile can be obtained during flight; The initial value of the Euler angles is determined by the initial flight conditions; Angle velocities are placed based on Equation (21-23), which includes both rigid and flexural body expressions, so at Euler angles there is the effect of deformation of the structure, hence its value in rigid projectile simulations. Flexibility can vary Euler angles values, as shown in the results section (Figure 5); Incidentally, this is one of the important effects of aeroelasticity on the flight path of the projectiles.

$$\begin{Bmatrix}\dot{\phi}\\ \dot{\theta}\\ \dot{\psi}\end{Bmatrix}=\begin{bmatrix}1 & sin\,\phi\,tan\,\theta & cos\,\phi\,tan\,\theta\\ 0 & cos\,\phi & -sin\,\phi\\ 0 & sin\,\phi\,sec\,\theta & cos\,\phi\,cos\,\theta\end{bmatrix}\begin{Bmatrix}P\\ Q\\ R\end{Bmatrix} \quad (45)$$

Where the quantities $(\dot{\phi}\ \dot{\theta}\ \dot{\psi})$ represent the rate of Euler angles; However, in simulations, due to problems with Euler's angle calculations, quatrains are used for orientation calculations, the description of which is beyond the scope of this article.

Modeling, simulation and validation

Flight equations modeling has been done in Simulink environment of MATLAB software, which uses its capabilities such as: look up tables, display tools, input and output monitoring tools, coding blocks, module writing, etc. Simulation validation And the input\outputs observation of different parts of the simulation is easier by Simulink; In the software model, the different parts of the code are separated into blocks with specific names; Software blocks include blocks: dynamic equations, environmental conditions, aerodynamic loads, wind-body angles, forces and moments, generalized loads, stability criteria, dynamic stresses and strains; The following figure shows a section of the home page of a flexible projectile flight simulation software that some pointed blocks is observable.

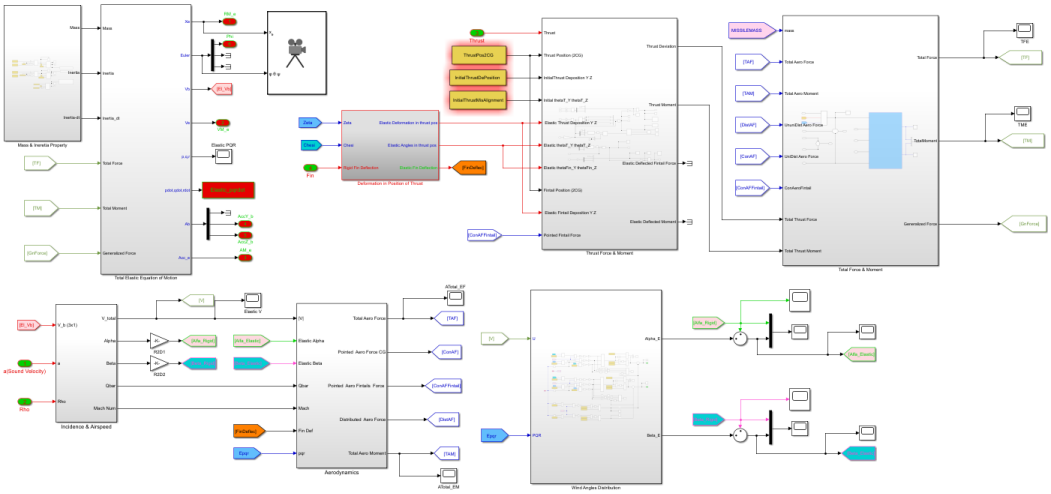

Figure 5 Displays a section of the blocks of home page of flexible projectile flight simulation software; Blocks of equations of motion and orientation, calculation of aerodynamic loads, effect of propulsion's deflection, generalized loads and the resultant of forces and moments are known. Each of these blocks also contains a large number of block diagrams, look up tables, and interface codes.

Software and simulation validation are considered in several areas; As validation of input parameters can include the validation of aerodynamic coefficient distribution, mass distribution, stiffness, natural frequencies and vibration modes; Regarding the validation of aerodynamic coefficients As described above, the integral of the force coefficient distribution and its torque integral around the center of mass must be equal to the aerodynamic coefficients in the rigid state; The following figure shows the distribution of vertical bending coefficients in terms of different attack angles along the structure that its integral and torque relative to the center of mass of each must be equal to the number of vertical bending coefficient and the corresponding aerodynamic torque coefficient in the rigid geometry model. The

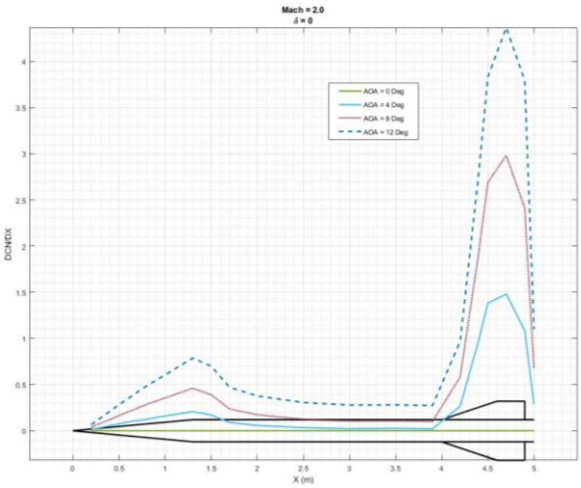

Figure 6 shows the distribution of vertical bearing coefficients in terms of different attack angles along the structure.

Structure frequencies and shape modes are determined by numerical methods (in this paper by Galerkin's Method) and validate by modal tests; Code validation is also discussed in the areas of implementation of equations of motion, orientation, flight path, calculation of aerodynamic and generalized loads; The equations of motion, orientation, flight path, and aerodynamic loads are determined by using standard flight tests and comparison with rigid projectile simulation; The validation of generalized coordinates is also measured by airborne vibration sensors, in which case the frequency and amplitude of the generalized coordinates obtained from the simulation must match the number measured from the airborne sensors in amplitude and frequency.

It is necessary to mention, in following results, flexibility of aerodynamic surfaces is not modeled; It also is assumed that the structure has a reasonable thickness to withstand the loads on the structure, that is, the rupture does not occur due to exerted loads.

Results & Discussions

Based on the extracted equations of motion for flexible projectile, it is possible to guess: structure thickness which can also represent the structure's natural frequency , the curve function of the thrust force (assuming the specific impact is constant), initial error in thrust force (deflection and out-centering), angular velocities, velocity of the projectile especially when the propulsion is switched off and control commands etc. can be effective in differentiating the results of flexible projectile simulation with rigid type.

Thrust vector moment occurs due to inherent deviation, deformation of the structure or both; In the rigid simulation, If is considered the propulsion vector have no inherent or initial deviation (like deviation and out-centering), the moments and lateral forces resulting from the propulsion deviation are zero, however in the flexible projectile simulation is not zero due to lateral deformations of the structure; Under normal conditions, due to small amount of the transverse loads on the projectile, the deformations and deviations of the structure at the outlet of the thrust force are negligible, so it is expected that the amount of the generated moments and therefor the difference between the rigid and flexible projectile simulations be little.

Thrust deviations caused by inherent deviations or structure's deformations due to lateral loads or both; if there is no initial deviation in thrust force, often amount of the exerted lateral forces on the body is low and therefor the results of two simulations are almost coincident (Figure 7); Although there is a slight difference in the flight path; It is obvious that the amount of lateral loads depends on aerodynamic factors (aerodynamic pressure and geometry), guidance and control commands and the inherent deviation of the propulsion. It can be said that in the ballistic flight where the projectile is simulated with no guidance commands, the main factor that causes the difference between the results of the two simulations is due deviations of the of propulsion which its effects is more than the effects of velocity and aerodynamics pressure.

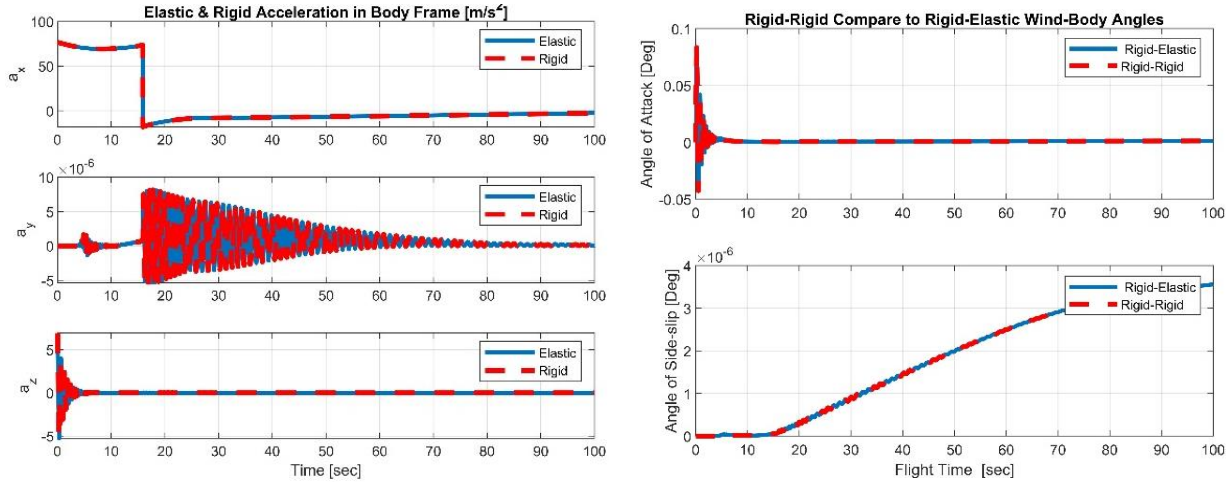

Figure 7 Wind-body angles and linear acceleration in the body frame coordinate in simulations of rigid and flexible projectile (in the absence of thrust vector moment due to body deformation, little difference is seen in the results).

A) Simulation of rigid and flexible projectile by considering the moment of the thrust vector due to body deformation

In this case, considering the moment generated due to the deformation of the body at the position of the nozzle outlet, the difference between the results of the two rigid and flexible projectile simulations with each other is became more obvious; The differences between two simulations can be seen, at least momentarily, even in situations where the stiffness of the body is high, due to the great magnitude of propulsion force (Figure 8); By the way, since the projectile is modeled as a ballistic launch vehicle without any external stimulation, the created vibrations and induced lateral accelerations are damped due to the structural depreciation and flight stability of the projectile and finally two simulations will match to each other.

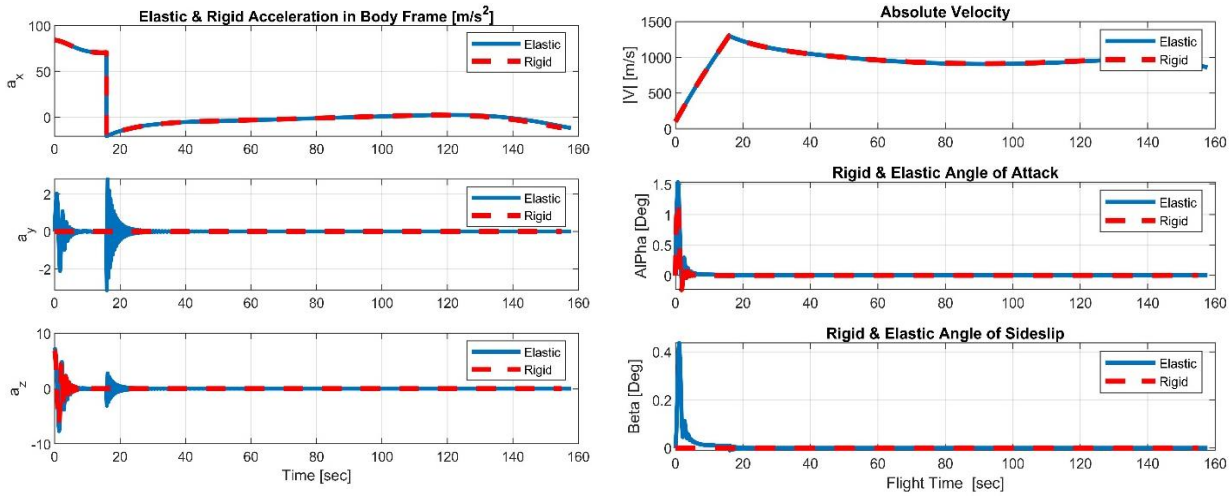

Figure 8 Wind-body angles and linear acceleration in the body coordinate system in simulations of rigid and flexible projectile (Because of deviation in thrust vector and body deformation & vibration), two jumps observe in transverse acceleration in moment of turning on and off the propulsion).

As can be seen from Figure (9), increasing the initial velocity decreases the transverse acceleration in x-y plane of the projectile due to increase of axial momentum and then it's stability when the propulsion is turned on and increases when it is turned off; Increasing the initial velocity has tripled the amount of transverse acceleration of the projectile at the time of shutdown; It should be noted, however, that these changes also depend on the aerodynamic geometry, distribution of aerodynamic coefficients, and stiffness along the projectile structure.

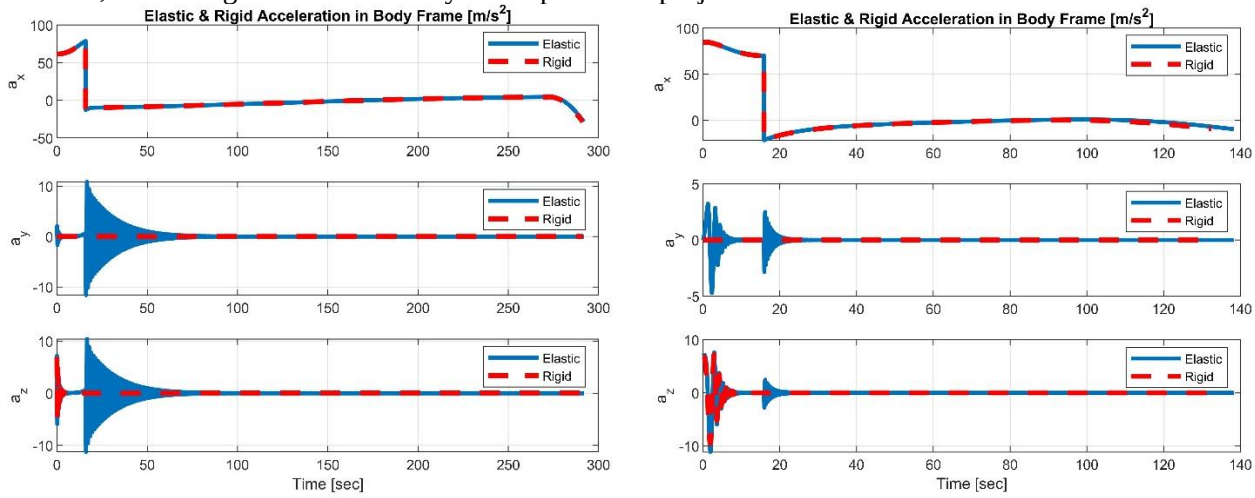

Figure 9 Values of linear acceleration in the body in simulations of rigid and flexible projectile for two cases of $\boldsymbol{V_0 = 10\frac{m}{s}}$ (right) and $\boldsymbol{V_0 = 1000\frac{m}{s}}$ (left) when the propulsion turns on.

As can be seen from Figure (10), increasing of the velocity at time of thrust becomes on, increases the transverse acceleration due to the shutdown of the propulsion; However, the low speed at the moment of applying the propulsion has caused more initial deviation (because of little amount of the momentum in x_B direction), which has ultimately resulted in a greater miss in the trajectory and lower collision accuracy or CEP; Although the range of the projectile has increased due to the increase in the initial velocity. It should be noted that this initial velocity related to stage of projectile, velocity of launching board or just as conceptual design and evaluating criteria. Also, this increase in velocity is to be increased to such an extent that, after the propulsion is completed, the velocity of the projectile is somewhat less than the velocity of the flutter instability.

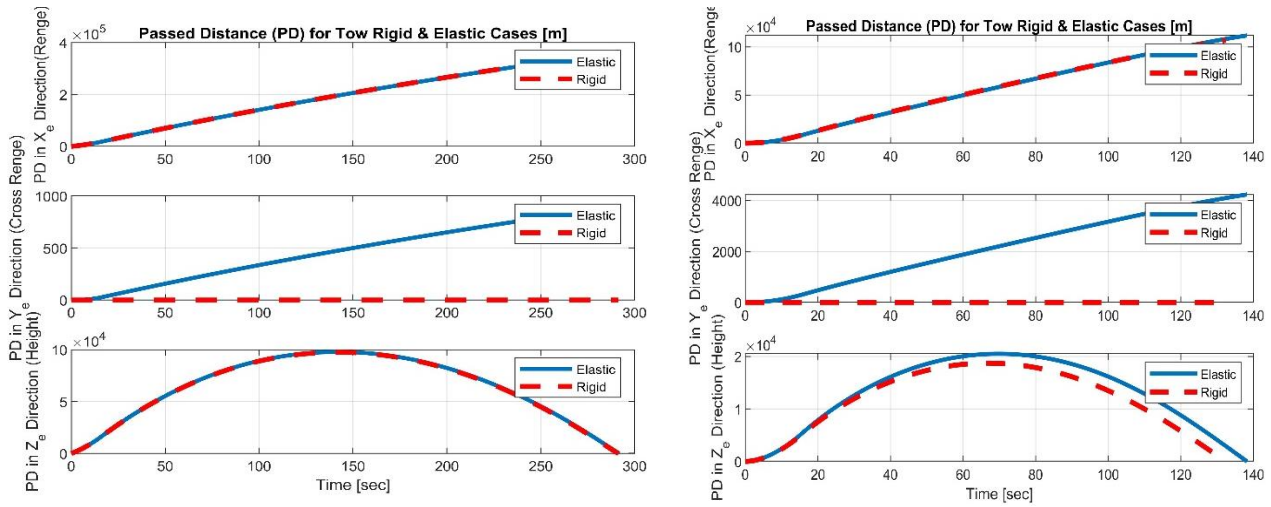

Figure 10 Values of linear acceleration in the body coordinate in simulations of rigid and flexible projectile for two cases of $\boldsymbol{V_0 = 10\frac{m}{s}}$ (right) and $\boldsymbol{V_0 = 1000\frac{m}{s}}$ (left) when the propulsion turns on.

B) Changing in Propulsion curve function by keeping specific impulse (Isp) constant

The curve and timing of the propulsion force can be changed to investigate the role of the propulsion model. It is predicted that by decreasing the propulsion burning time while it's Isp, is constant, the effects of aeroelasticity such as induced transverse accelerations, unwanted angular velocities and directional angles, and the elastic portion of the wind-body angles will increase, especially when the rocket motor is switched on or off. However, the difference in flight paths and the miss distance cannot be easily judged, because the structure's natural frequency increases due to tensile axial force at most length of the projectile cause by burning of the propellant; But at least it can be said that the amount of difference between the two simulations of rigid and flexible projectiles increases in the same time interval of the simulation; furthermore reducing the burning time will result in a maximum velocity at a lower altitude and therefore increase the aerodynamic pressure as one of the important factors in the occurrence of aeroelastic instability.

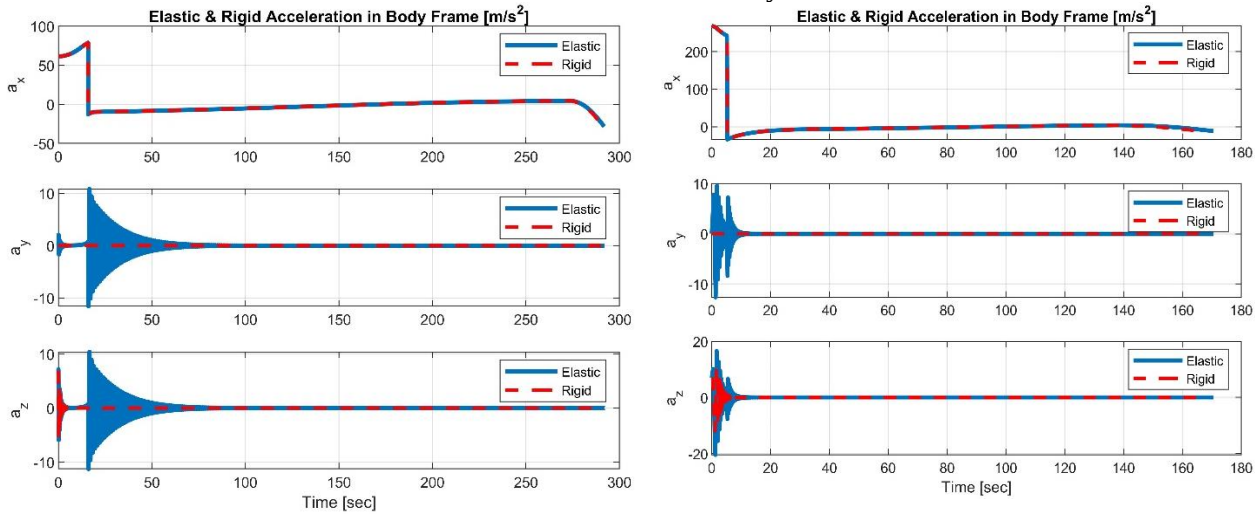

Figure 11 Linear Acceleration in body frame coordinate in simulations of rigid and flexible projectile for two cases $\boldsymbol{V_0 = 10\ \frac{m}{s}}$ (right) and $\boldsymbol{V_0 = 1000\ \frac{m}{s}}$ (left) Assuming the propulsion time is halved.

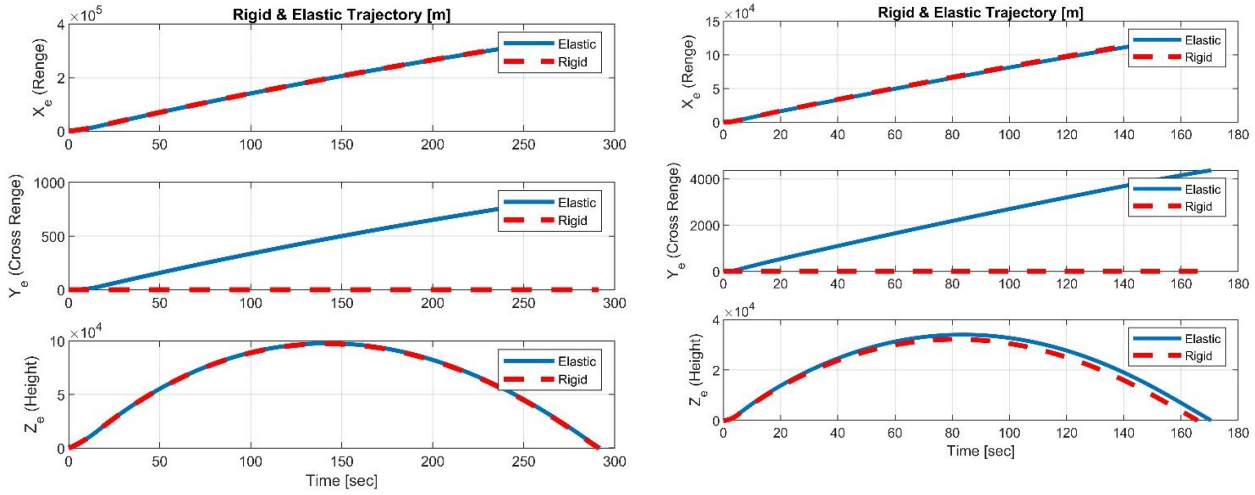

Figure 12 Flight path (Trajectory) in simulations of rigid and flexible projectile for two cases $\boldsymbol{V_0 = 10\ \frac{m}{s}}$ (right) and $\boldsymbol{V_0 = 1000\ \frac{m}{s}}$ (left) Assuming the propulsion time is halved

C) Investigating the effect of rolling command

As seen in the flexible projectile equations of motion (Equations 21 to 25), the angular velocities have a direct role in increasing the effects of flexibility on the flexible projectile dynamics, so it is expected that differences between two rigid and flexible simulations increase.

Since the value of the angular velocity around the longitudinal axis (rolling angular velocity) is often greater than the other two angular velocities (pitching and yawing), is used a stable rolling velocity by means of a constant deflection of the control surfaces to investigate this; It is expected that if the rolling velocity exceeds a certain quantity, it can cause aeroelastic instability of the projectile, which can be seen in the figure (Figure 15) in the divergence of the values of the wind-body angles; According to (Figure 13), the increase in aeroelasticity effects due to the rolling velocity has caused a difference in the values of the pitch and yaw angles in the two simulations of rigid and flexible projectiles. In the no-roll mode (Figure 13 on the right), the value of the projectile roll angle was constant during flight time and the difference between the results of the two simulations was due to the effects of inherent and deformation-related deflection of the propulsion.

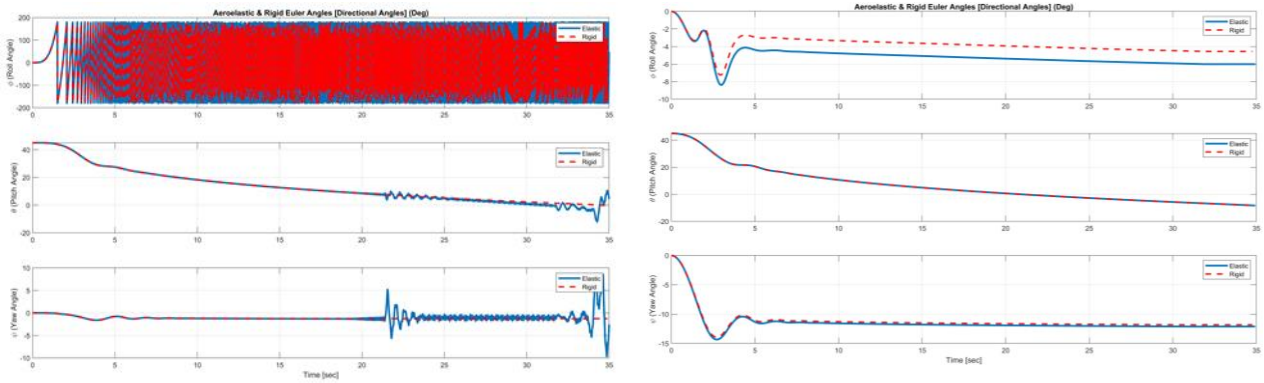

Figure 13 Euler's angles in two simulations of rigid and flexible projectile for two cases: without roll command and stable (right) with roll command and unstable (left).

As can be seen in (Figure 14), the aileron command increases the lateral acceleration exerting to the structure, which is not seen in rigid simulation of the projectile; due to increasing in amount of the induced wind body angles and finally increase the aerodynamic loads on the structure; In addition to

these, the fact that more deformations of the structure, the amount of transverse loads due to the deflection of the propulsion vector also increases.

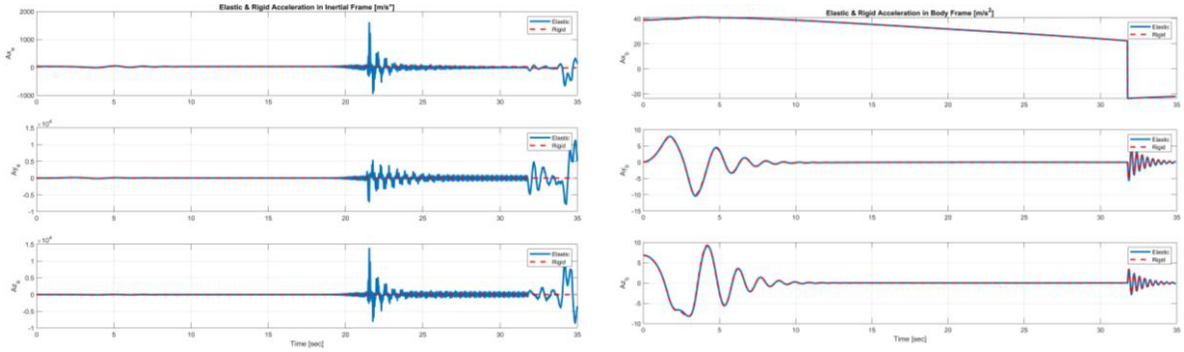

Figure 14 Linear Acceleration on body coordinate in two simulations of rigid and flexible projectile for two cases: without roll command and stable (right) with roll command and unstable (left).

As can be seen in (Figure 15) for the case where the angular velocity of the projectile is zero or insignificant, there is no significant difference in the values of the wind-body angles (right); However, with the presence of angular velocity, the difference between the wind-body angles of the two rigid and flexible simulations has increased, so that if it increases too much, it will cause divergence and instability in flight situation.

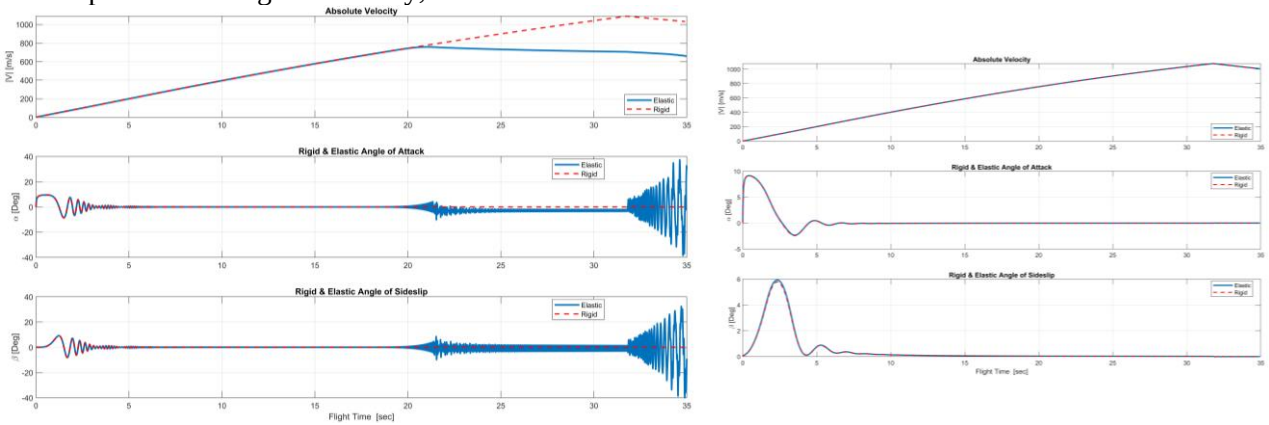

Figure 15 Wind-body angles in two simulations of rigid and flexible projectile for two cases: without roll command and stable (right) with roll command and unstable (left).

One of the cases that occurs during aeroelastic instabilities of flexible projectiles is the increase of the contribution of the elastic portion of the wind-body angles and divergence in its amount; In most cases when the projectile is stable, the contribution of the expressions resulting from the deformation (elastic portion) is insignificant compared to the rigid portion of the wind-body angles; As instability tends to occur, deformations of the structure i.e. generalized coordinates increases, therefore the contribution of the elastic component increases and overcomes the rigid portion and eventually goes toward divergence.

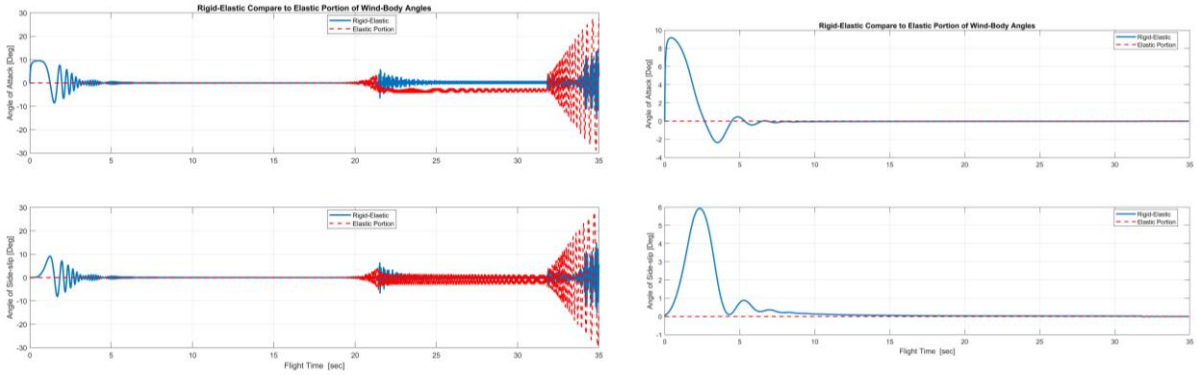

Figure.16 Rigid and elastic portion of wind-body angles for elastic projectile With First Mode 12Hz without roll command in stable state (right) and with **2°** Aileron command and in instable position (left).

Conclusions

As shown in this study, the effects of structural flexibility are usually significant for projectiles with a slenderness ratio greater than 15, therefore they have low body's natural frequency (less than 20 Hz); In a conventionally designed projectile with a slenderness ratio of less than 15, aeroelastic effects seldom cause flight instability; Because in practice, due to the large natural frequency, lack of control commands and low wind-body angles, small angular velocity, aeroelasticity only changes the flight quantities and changes the range and accuracy of the projectile, not cause to instability; In such cases, the only important factor in projectile instability is the inherent deflection and decentering of the propulsion vector, In the presence of flexibility, its effects can be intensified; In this regard, it was shown that by increasing in structure's flexibility and value of the initial error in thrust force (either from out-centering or deflection), differences between rigid and flexible projectile simulations increase; In this regard, the effect of body deformation on intensify of inherent deflection of propulsion as well as on the stability and flight conditions of the flexible projectile were evaluated. It was also shown that rigid simulation lacks the ability to investigate the effects of the propulsion vector curve and the natural frequency of the structure on flight stability; Also, the effects of rolling angular velocity on increasing the share of flexibility-dependent quantities and the difference between the results of two rigid and flexible projectile simulations was shown;

It also was shown that with the help of simulation tool, the flight behavior of the aircraft can be reviewed on some design inputs such as stiffness distribution of structure, curve of the thrust force and its inherent deviation & out-centering, flight speed, spinning velocity etc.; then used these results to optimize design parameters before field tests. it was shown that spinning velocity, body stiffness (natural frequency) and the inherent values of deflection and out-centering of the thrust force have a major effect on the stability of the projectile and with the help of simulation one can find suitable range for each of them according to the design goals and using them to extract the system requirements.

References

[1] U. La Roche and H. L. La Roche, "Induced Drag Reduction Using Multiple Winglets, Looking Beyond the Prandtl-Munk Linear Model," in 2nd AIAA Flow Control Conference, 2004, p. 2120.

[2] D. Bushnell, "Aircraft drag reduction—a review," Proceedings of the Institution of Mechanical Engineers, Part G: Journal of Aerospace Engineering, vol. 217, no. 1, pp. 1-18, 2003.

[3] J. D. Anderson Jr, Fundamentals of aerodynamics. Tata McGraw-Hill Education, 2010

[4] K. A. Al Sidairi and G. Rameshkumar, "Design of Winglet Device for Aircraft," International Journal of Multidisciplinary Sciences and Engineering, vol. 7, no. 1, 2016.

[5] M. A. Cancino Queirolo, "Impact of Morphing Winglets on Aircraft Performance," 2018.

[6] P. Pragati and S. Baskar, "Aerodynamic analysis of blended winglet for low speed aircraft," in Proceedings of the World Congress on Engineering, 2015, vol. 2.

[7] M. H. Sohn and J. W. Chang, "Visualization and PIV study of wing-tip vortices for three different tip configurations," Aerospace Science and Technology, vol. 16, no. 1, pp. 40-46, 2012.

[8] P. Paudel, "Aerodynamic aspects in the development of morphing winglet for a regional aircraft," Dept. App. Sci. Aerospace. Eng. Ryerson University, 2013.

[9] H. S. Helal, E. E. Khalil, O. E. Abdellatif, and G. M. Elhariry, "Aerodynamic Analyses of AircraftBlended Winglet

Performance," IOSR J. Mech. Civ. Eng. Ver, vol. 13, no. 3, pp. 2320-334, 2016.
[10] J. Halpert, D. Prescott, T. Yechout, and M. Arndt, "Aerodynamic optimization and evaluation of KC- 135R winglets, raked wingtips, and a wingspan extension," in 48th AIAA Aerospace Sciences Meeting Including the New Horizons Forum and Aerospace Exposition, 2010, p. 57.
[11] N. N. Gavrilović, B. P. Rašuo, G. S. Dulikravich, and V. B. Parezanović, "Commercial aircraft performance improvement using winglets," FME Transactions, vol. 43, no. 1, pp. 1-8, 2015.
[12] G. Narayan and B. John, "Effect of winglets induced tip vortex structure on the performance of subsonic wings," Aerospace Science and Technology, vol. 58, pp. 328-340, 2016.
[13] M. A. Azlin, C. M. Taib, S. Kasolang, and F. Muhammad, "CFD analysis of winglets at low subsonic flow," in Proceedings of the World Congress on Engineering, 2011, vol. 1, pp. 6-8.
[14] J. C. Patterson Jr, "Wingtip Vortex Turbine," ed: Google Patents, 1990.